Computer Assisted Methods in Engineering and Science
30(4): 481–503, 2023, doi: 10.24423/cames.1016

Modeling of Cracking of the Concrete Cover Taking into Account the Coupled Diffusion/Mechanical Process

Kseniya YURKOVA, Tomasz KRYKOWSKI*

Department of Mechanics and Bridges, Faculty of Civil Engineering, Silesian University of Technology, Gliwice, Poland; e-mail: kseniya.yurkova@polsl.pl

** Corresponding Author e-mail: tomasz.krykowski@polsl.pl*

This paper presents a mechanical-diffusion one-way coupled corrosion model that allows the analysis of both accelerated and natural reinforcement corrosion. The impact of corrosion products on the concrete cover is exerted using the tensor of the volumetric strain rate dependent on the rate of concentration change of corrosion products or the rate of concentration change of ferrous ions. The approach proposed in the paper enables the analysis of the impact of corrosion products with a complex composition that depends on the intensity and density of the electric current. The model also enables the analysis of cases where the distribution of corrosion products is inhomogeneous around the circumference of the rebar.

Keywords: corrosion, FEM, elastic-plastic, cover cracking.

1. Introduction

Reinforcement corrosion is one of the leading causes of the destruction and degradation of reinforced concrete structures [1]. The appropriate approach to this problem at the design stage of the structure is a guarantee of its economical exploitation throughout its lifetime [2, 3].

Classical models of analysis of the reinforced concrete degradation concern, in the vast majority of the cases, the so-called thick-walled cylinder models. The study of Bažant [4] or the works of [5, 6] can be mentioned here. A very thorough review of this type of models can be found in [7], which refers to the advantages and disadvantages of this type of methods for estimating cover degradation.

More advanced models take into consideration the accumulation of corrosion products in the empty pore spaces in the transition layer and the transfer of

the products through the crack outside the cover of concrete. The phenomenon of the deposition of corrosion products in the transition layer with increased porosity was first reported in [8], and the concept of the so-called corrosion products accommodation area, i.a., in [9, 10]. The authors in [11] described the effective impact of corrosion products on the concrete cover (in the case of accelerated corrosion), taking into account their transfer through cracks to the environment.

A very important development of the classical models is the attempt to take into account temperature, moisture and concentration of aggressive substances, such as e.g., chloride ions or carbon dioxide [12, 13]. Despite including additional physical fields in a more or less detailed way, these papers treat the problem of reinforcement corrosion in a manner similar to the solution that is the basis for formulating analytical models. Within this group, one can mention works in which a very advanced FEM model is used to model thermo-mechanical issues and problems of transporting aggressive substances, while the bar corrosion process itself is based on the classical approach assuming an increase in the volume of the reinforcing bar [14–16].

Another step aimed at improving the cover degradation forecasting models is the attempt to formulate an approach that includes the heterogeneous distribution of corrosion products on the circumference of the rebar, as well as the attempts to modify the approach to estimating the impact of corrosion products on concrete. Within the first group, the following papers should be mentioned [17–19], as well as the models treating the concrete cover as a mesoscale media [20, 21]. The second group includes papers [22] describing the problem of corrosion with the use of modified elements of the cohesive type or an approach based on the tensor of the rate of equivalent volumetric strain [23]. The latter work also includes the change in the effective impact of corrosion products on the concrete cover as a result of pushing the corrosion products outside through the cracks or the interactions resulting from the differences between the mass loss calculated gravimetrically and theoretically determined from Faraday's law in the tests of accelerated corrosion [24].

In the process of the corrosion of the reinforcement, iron ions are transferred to the pore solution, and corrosion products are transported to the deeper layers of the concrete cover. Attempts to model such issues were formulated, among others, in [25, 26]. In [27], a model of a transition zone with mechanical parameters modified as a result of penetration by reinforcement corrosion products was proposed.

Despite the often-complex approach to describing the issues of cover degradation, the aforementioned models treat the increase in product volume as a mechanical problem. This results in enforcing substitute statically equivalent volumetric strains that map the interactions between corrosion products. It is over-

looked that the loss of iron ions and the process of rust growth are mutually coupled and should be described as a diffusion-mechanical problem dependent on the electric current.

In this paper, a new model is formulated that enables the analysis of the coupled mechanical-diffusion problem of concrete cover degradation as a result of reinforcement corrosion. The three elements in the approach to the problem are new. The problem of corrosion is treated in the model as a problem described by the diffusion equations, with the source being a function of the electric current. The mechanical interactions are formulated by the rate of the volumetric strain tensor dependent on the rate of the concentration of corrosion products (the model allows for a comprehensive approach to modeling issues with both homogeneous and inhomogeneous distribution of products on the circumference of rebar). The model additionally enables the analysis of the cases in which corrosion products are a mixture of many phases of various oxides, hydroxy oxides and oxyhydroxides.

2. Mathematical model

2.1. Introduction

The model of a multicomponent elastic-plastic medium with diffusion is analyzed. In the model, four components are distinguished, i.e., skeleton α_0, iron ions α_1, reinforcement corrosion products α_2 and other substrates of the electrochemical reaction necessary for its proper course α_3. It was assumed that the reinforcement corrosion process would be forced artificially with the help of an external electric field (electrolysis process). An external source of electric current, in accordance with Faraday's law, forces the migration of iron ions into the pore solution (the model lends itself to the analysis of natural reinforcement corrosion initiated by the environment interaction). The formulation of constitutive relationships and equations describing the process of accelerated corrosion was based on the classical theory, ignoring electrical interactions. Both the electromechanical interactions caused by the Lorenz force present in the momentum balance equation and the dot product of vector of the electric current density, as well as the electrostatic field intensity $\mathbf{iE}$ have been omitted in the energy balance equation [28, 29]. It was assumed that corrosion effects are defined by appropriately defined mass sources.

From the point of view of thermomechanics of multicomponent media, the equations of the elastoplastic medium with diffusion have been described in many scientific publications [28, 30–33]. In the subsequent points, the considerations refers to the essential elements of the theory, omitting detailed considerations that can be found in the previously mentioned literature on the subject.

2.2. Assumptions of the theory of multicomponent media with a dominant component

A multicomponent medium containing α components, $\alpha = 0..3$ with masses m_α the density of the mixture component ρ_α and the concentration of the mixture component c_α [30]:

$$\rho_\alpha = \frac{m_\alpha}{V}, \quad c_\alpha = \frac{\rho_\alpha}{\rho}, \quad \rho = \sum \rho_\alpha, \tag{1}$$

where $V \equiv V_\alpha$ is the volume of the considered phase of the mixture (overlapping continua).

According to the theory of mixtures [31], the velocity of the mixture component is described by the equation:

$$\mathbf{v}_\alpha = \mathbf{u}_\alpha - \mathbf{v}, \quad \rho\mathbf{v} = \sum \rho_\alpha \mathbf{v}_\alpha, \tag{2}$$

where $\mathbf{v}_\alpha$ is the velocity of the mixture component, $\mathbf{u}_\alpha$ is the diffusion velocity of the component, and $\mathbf{v}$ is the average velocity.

The theory of mixtures with the so-called dominant component assumes that the density of the skeleton is much higher than the density of the remaining components of the mixture $\rho_0 \gg \rho_\alpha$ which implies the fulfillment of two relationships [30]:

$$\rho = \sum \rho_\alpha \cong \rho_0, \quad \rho\mathbf{v} = \sum \rho_\alpha \mathbf{v}_\alpha \cong \rho_0 \mathbf{v}_0. \tag{3}$$

2.3. Mass balance equation

Mass balance equations can be defined by relationships [30, 34]:

$$\frac{\partial \rho_\alpha}{\partial t} + \operatorname{div}(\mathbf{J}_\alpha) = R_\alpha, \quad \mathbf{J}_\alpha = \rho_\alpha \mathbf{v}_\alpha = \mathbf{j}_\alpha + \rho_\alpha \mathbf{v}, \quad \mathbf{j}_\alpha = \rho_\alpha \mathbf{u}_\alpha, \quad \alpha = 0...3, \tag{4}$$

where ρ_α is the partial mass density of the mixture component, $\mathbf{J}_\alpha$ is the mass flux of the component, and $\mathbf{j}_\alpha$ is the diffusion mass flux of the component.

In this study, we refer in detail to two components important for modeling the reinforcement corrosion process. These components are iron ions $\alpha = 1$, migrating to the solution as a result of iron dissolution under the influence of an external source of electric current applied to the system (electrolysis process) and reinforcement corrosion products $\alpha = 2$. It is assumed that both the ratio of mass (density) of corrosion products and iron ions [5] and their velocity are constant values for a given value of electric current intensity (and density) ($\alpha = \alpha(I) = \text{const}$, $\vartheta = \vartheta(I) = \text{const}$):

$$\frac{\dot{m}_1}{\dot{m}_2} = \frac{\dot{m}_{\mathrm{Fe}^{2+}}}{\dot{m}_{cp}} = \alpha, \quad \frac{\dot{\varrho}_1}{\dot{\varrho}_2} = \frac{\dot{\varrho}_{\mathrm{Fe}^{2+}}}{\dot{\varrho}_{cp}} = \vartheta, \quad \dot{m}_1 = \dot{m}_{\mathrm{Fe}^{2+}} = k_{\mathrm{eff}} I, \quad \dot{m}_2 = \frac{\dot{m}_1}{\alpha}, \tag{5}$$

where $\dot{m}_1 \equiv \dot{m}_{\mathrm{Fe}^{2+}}$ is the rate of mass of iron ions (according to Faraday's law of electrolysis), $\dot{m}_2 \equiv \dot{m}_{cp}$ is the rate of mass of corrosion products, α and ϑ are material constants depending on the composition of corrosion products, k_{eff} is effective electrochemical equivalent of iron, and I is electric current intensity.

When analyzing the problems of cover degradation as a result of corrosion, both the situation in which the composition of corrosion products is fixed and the situation in which the composition is variable and dependent on the corrosion current and time were considered.

The iron ion mass balance equation takes the form:

$$\rho \frac{dc_1}{dt} + \operatorname{div}(\mathbf{j}_1) = R_1, \quad R_1 = \frac{\dot{m}_1}{V}, \tag{6}$$

where c_1 is the concentration of ferrous ions, $\mathbf{j}_1$ is the diffusion mass flux of ferrous ions, R_1 is the mass source of ferrous ions, and $V \equiv V_\alpha$ is the volume of multicomponent media.

An analogous balance equation can be formulated for reinforcement corrosion products (component $\alpha = 2$). The mass balance equation of corrosion products takes the following form after taking into account dependence (5):

$$\rho \frac{dc_2}{dt} + \operatorname{div}(\mathbf{j}_2) = R_2, \quad R_2 = \frac{\dot{m}_2}{V} = \frac{\dot{m}_1}{\alpha V}, \tag{7}$$

where c_2 is the concentration of corrosion products, $\mathbf{j}_2$ is the diffusion mass flux of corrosion products, and R_2 is the mass source of corrosion products.

2.4. Constitutive relationships

Constitutive relationships in the mechanical-diffusion model, thermodynamic constraints related to the dissipation of internal parameters and their evolution equations in a multi-component medium with a dominant constituent takes the form [31, 32]:

- Constitutive relationships:

$$\boldsymbol{\sigma} = \rho \frac{\partial A}{\partial \boldsymbol{\varepsilon}^e}, \quad M_\alpha = \frac{\partial A}{\partial c_\alpha}, \tag{8}$$

  where A is Helmholtz free energy, $\boldsymbol{\sigma}$ is the stress tensor, $\boldsymbol{\varepsilon}^e$ is the elastic strain tensor and M_α is the chemical potential [30];

- Dissipation inequality:

$$\boldsymbol{\sigma} : \dot{\boldsymbol{\varepsilon}}^p - \mathbf{X}^\omega \dot{\boldsymbol{\omega}} - \sum_\alpha \mathbf{j}_\alpha \operatorname{grad} M_\alpha \geq 0, \quad \mathbf{X}^\omega = \rho \frac{\partial A}{\partial \boldsymbol{\omega}}, \tag{9}$$

  where $\boldsymbol{\varepsilon}^p$ is the plastic strain tensor, $\boldsymbol{\omega}$ is the internal parameter describing the hardening and softening of material, and $\mathbf{X}^\omega$ is the thermodynamic force;

- Equations describing the evolution of thermodynamical fluxes:

$$\dot{\boldsymbol{\varepsilon}}^p = \gamma \frac{\partial G}{\partial \boldsymbol{\sigma}}, \quad -\dot{\boldsymbol{\omega}} = \gamma \frac{\partial G}{\partial \mathbf{X}^\omega}, \quad -\mathbf{j}_\alpha = \mathbf{K} \operatorname{grad} M_\alpha, \tag{10}$$

where G is plastic potential.

Taking into account in Eq. (6), the Helmholtz free energy, which after expanding and omitting irrelevant elements, can be written in the form:

$$\rho A\left(c_\alpha, \boldsymbol{\varepsilon}^e, \boldsymbol{\omega}\right) = \frac{1}{2}\boldsymbol{\varepsilon}^e : \mathbf{C}^e : \boldsymbol{\varepsilon}^e - \sum_\alpha \boldsymbol{\varepsilon}^e : \mathbf{C}^e : \boldsymbol{\xi}_\alpha \left(c_\alpha - c_0\right) + A_p\left(\boldsymbol{\omega}\right), \tag{11}$$

the constitutive equations can be formulated.

The equations of the model describing the evolution of the stress tensor $\boldsymbol{\sigma} = \boldsymbol{\sigma}\left(\boldsymbol{\varepsilon}^e, \boldsymbol{\varepsilon}_\alpha^V\right)$ and the chemical potential $M_\alpha = M_\alpha\left(c_\alpha, \boldsymbol{\varepsilon}^e, \boldsymbol{\omega}\right)$ can have the following form:

$$\boldsymbol{\sigma} = \mathbf{C}^e : \boldsymbol{\varepsilon}^e - \sum_\alpha \mathbf{C}^e : \boldsymbol{\xi}_\alpha \left(c_\alpha - c_{\alpha,0}\right) = \mathbf{C}^e : \left(\boldsymbol{\varepsilon} - \boldsymbol{\varepsilon}_\alpha^V\right), \quad \boldsymbol{\varepsilon} = \boldsymbol{\varepsilon}^e + \boldsymbol{\varepsilon}^p, \tag{12}$$

$$\boldsymbol{\varepsilon}_\alpha^V = \boldsymbol{\xi}_\alpha \left(c_\alpha - c_{\alpha,0}\right), \quad M_\alpha = M_\alpha\left(c_\alpha, \boldsymbol{\varepsilon}^e, \boldsymbol{\omega}\right) = \frac{\partial A\left(c_\alpha, \boldsymbol{\varepsilon}^e, \boldsymbol{\omega}\right)}{\partial c_\alpha}, \tag{13}$$

where $\boldsymbol{\varepsilon}_\alpha^V$ defined in relation (13) is the tensor of the volumetric strains caused by the change in the concentration of the c_α in the considered region.

The tensor of volumetric strains resulting from the change in the concentration of corrosion products in the problems of computer modeling of the cover can be conveniently formulated in the velocity form $\dot{\boldsymbol{\varepsilon}}_2^V$ depending, among other things, on the intensity of the electric current. This type of relationship was formulated in [23, 35]. In the case of corrosive interactions in a plane perpendicular to the axis of the rebar, the nonzero coordinates of the tensor take the form

$$\dot{\varepsilon}_{\gamma\delta}^V = \dot{\varepsilon}^V \delta_{\gamma\delta}, \quad \dot{\varepsilon}^V = \frac{(1-\beta)}{\eta \varrho_1 V_0} \frac{(\vartheta - \alpha)}{\alpha} \dot{m}_1, \quad \gamma, \delta = 1, 2, \tag{14}$$

where β is the parameter of the intensity of the interactions of corrosion products on the concrete cover, and V_0 is the volume of the region where the volume of corrosion products increases.

Equation (14) can be formulated depending on the rate of change of the concentration of iron ions $\dot{c}_1$ as well as the rate of change of the concentration of corrosion products $\dot{c}_2$. By taking into account Eq. (1) in Eq. (14), it is possible to formulate a dependence describing the evolution of the volumetric strain rate caused by corrosion products. The evolution of volumetric strains caused by the

increase in the volume of corrosion products can be associated with both the loss of iron ions and the increase in the volume of corrosion products:

$$\dot{\varepsilon}^V = \frac{(1-\beta)}{\eta \varrho_1 V_0} \frac{(\vartheta - \alpha)}{\alpha} V \rho \dot{c}_1,\ \dot{c}_1 = \frac{\dot{m}_1}{V\rho}, \tag{15}$$

$$\dot{\varepsilon}^V = \frac{(1-\beta)}{\eta \varrho_1 V_0} (\vartheta - \alpha) V \rho \dot{c}_2,\ \dot{c}_2 = \frac{\dot{m}_2}{V\rho}. \tag{16}$$

2.5. Modeling the composition of corrosion products on the surface of the reinforcement

In the cases when we are dealing with an accelerated corrosion process of reinforcement, the composition of the resulting products is complex and depends on the intensity and density of the current. In [36], the chemical composition was analyzed in the process of accelerated corrosion of reinforcement for a small range of corrosion current densities. The obtained chemical composition of the products was a mixture of iron oxides: FeO, Fe_2O_3, Fe_3O_4 and iron oxyhydroxides ($\alpha - FeO(OH)$, $\beta - FeO(OH)$, $\gamma - FeO(OH)$). In addition, the contribution of chemical compounds in the total mass of corrosion products is changed depending on the intensity (density) of the current in the system. It can be assumed that the total mass and density of corrosion products are expressed by the relationship:

$$m_R = \sum_x \xi_x m_x, \quad \varrho_R = \sum_x \xi_x \varrho_x, \quad \xi_x = \xi_x(i) = \xi_x(I), \tag{17}$$

where ξ_x is the percentage contribution of the chemical compound in the total mass (density) of corrosion products, m_x is the mass of the chemical compound, and ϱ_x is the specific density of the chemical compound.

Based on the results published [36], it was assumed that the percentage contribution of individual chemical compounds contained in corrosion products could be approximated using the logarithmic function (in the case of oxides) and the exponential function (in the case of oxyhydroxides). In addition, analogous functional relationships have been determined for the total percentage of oxides and oxyhydroxides in the mass of corrosion products:

$$\xi_x = \begin{cases} \ln(a_x i^{b_x}), & x = 1...4, \\ \exp\left(\dfrac{c_x i^{d_x}}{e_x i^{f_x}}\right), & x = 5...8, \end{cases} \tag{18}$$

where a_x and b_x are constants related to the percentage of oxides: FeO ($x = 1$), Fe_2O_3 ($x = 2$), Fe_3O_4 ($x = 3$), total oxide content ($x = 4$); however, c_x, d_x, e_x

and f_x are constants related to the percentage of oxyhydroxides: $\alpha-\mathrm{FeO(OH)}$ ($x = 5$), $\beta-\mathrm{FeO(OH)}$ ($x = 6$), $\gamma-\mathrm{FeO(OH)}$ ($x = 7$), total oxyhydroxides content ($x = 8$) in the total mass of corrosion products.

In the problems considered in the literature, the estimation of the impact of corrosion products on the cracking condition of the concrete cover is very often approached with the assumption that the corrosion products are a mixture of hydroxy oxides $\mathrm{Fe(OH)_2}$ and $\mathrm{Fe(OH)_3}$ [5, 8]. The parameters defining the evolution of the reinforcement corrosion process takes constant values in such a situation.

2.6. Yield surface and plastic potential in the Menetrey–Willam model

In the calculations of damage propagation in reinforced concrete elements, the elastic-plastic Menetrey–Willam (MW) material model with hardening/softening in compression and softening in tension (HSD2 model) implemented in the ANSYS program [37, 38] was used. The yield surface in this model is defined by the relationship [37]:

$$f_{\mathrm{MW}} = \frac{c_2}{c_3}\left[\frac{\sqrt{2}}{\sqrt{3}}I_1 + r\rho\right] + \rho^2 - \frac{1}{c_3}, \quad \rho = \sqrt{3J_2}, \quad I_1 = \mathrm{Tr}\,(\boldsymbol{\sigma}), \quad J_2 = \frac{1}{2}\mathbf{s}:\mathbf{s}, \tag{19}$$

where I_1 is the first invariant of the stress tensor $\boldsymbol{\sigma}$, J_2 is the second invariant of the deviator of stress tensor $\mathbf{s}$, r is a function of stress tensor invariants and material parameters, and c_2 and c_3 are values depending on the functions characterizing the hardening/softening of the material under compression Ω_c, tension Ω_t and material parameters.

The values c_2 and c_3 defining the yield surface (19) are defined by the following equations [37, 38]:

$$c_2 = \frac{1}{\sqrt{6}}\left[\frac{1}{\Omega_c f_c} - \frac{1}{\Omega_c f_b} + \frac{\Omega_c f_b - \Omega_{tc} f_t}{(\Omega_c f_c)^2}\right], \quad c_3 = \frac{3}{2}\frac{1}{(\Omega_c f_c)^2}, \tag{20}$$

$$r(\theta, e) = \frac{4\left(1-e^2\right)\cos^2\theta + (2e-1)^2}{2(1-e^2)\cos\theta + (2e-1)\left[4(1-e^2)\cos^2\theta + 5e^2 - 4e\right]^{0.5}}, \tag{21}$$

$$e = \frac{1+\epsilon}{2-\epsilon}, \quad \cos(3\theta) = \frac{3\sqrt{3}J_3}{2}\frac{1}{\sqrt{(J_2)^3}}, \tag{22}$$

$$\epsilon = \frac{\Omega_{tc} f_t}{\Omega_c f_b}\frac{(\Omega_c f_b)^2 - (\Omega_c f_c)^2}{(\Omega_c f_c)^2 - (\Omega_{tc} f_t)^2}, \quad \Omega_{tc} = \begin{cases} \Omega_t & \text{for } \kappa_c \le \kappa_{cm}, \\ \Omega_t\Omega_c & \text{for } \kappa_c > \kappa_{cm}, \end{cases} \tag{23}$$

where f_c is the compressive strength of the concrete, f_t is the tensile strength of the concrete, Ω_c is the function describing the mechanism of hardening and softening in compression, Ω_t is the function defining the mechanism of softening in tension, and κ is the internal parameter (equivalent plastic strain) in compression κ_c and tension κ_t.

The compression and tension hardening/softening functions used in the MW model (HSD2 model) are defined by Eqs. (24) and (25):

$$\Omega_c = \begin{cases} \Omega_{ci} + (1-\Omega_{ci})\sqrt{2\dfrac{\kappa}{\kappa_{cm}} - \dfrac{\kappa^2}{\kappa_{cm}^2}}, & \kappa < \kappa_{cm}, \\ 1 - (1-\Omega_{cu})\left(\dfrac{\kappa-\kappa_{cm}}{\kappa_{cu}-\kappa_{cm}}\right)^2, & \kappa_{cm} \le \kappa \le \kappa_{cu}, \\ \Omega_{cr} + (\Omega_{cu}-\Omega_{cr})\exp\left(2\dfrac{\Omega_{cu}-1}{\kappa_{cu}-\kappa_{cm}} \cdot \dfrac{\kappa-\kappa_{cu}}{\Omega_{cu}-\Omega_{cr}}\right), & \kappa_{cu} < \kappa, \end{cases} \tag{24}$$

$$\Omega_t = \exp\left(-\frac{\kappa}{a_t}\right), \quad a_t = \frac{g_{ft}}{f_t}, \quad g_{ft} = \max\left(\frac{G_{ft}}{L_i}, \frac{f_t^2}{E}\right), \tag{25}$$

where L_i is the effective length, E is Young's modulus, G_{ft} is the fracture energy, and κ_{cm}, κ_{cu}, Ω_{cr}, Ω_{tr} are the values characterizing the curves of hardening and softening in compression and tension, Fig. 1.

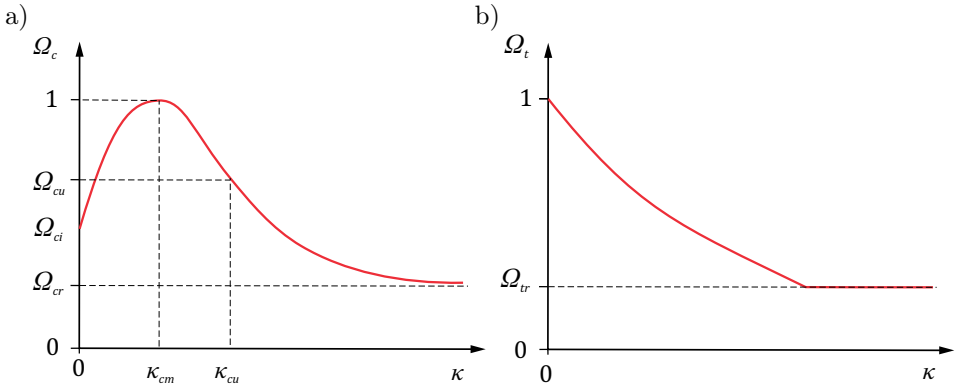

FIG. 1. Functions describing material: a) hardening and softening in compression Ω_c, b) softening in tension Ω_t.

Plastic potential $G = G_{\mathrm{MW}}$ in the MW model was defined by the relation [32, 38, 39]:

$$G_{\mathrm{MW}} = \rho^2 + B_g\rho + C_g\frac{I_1}{\sqrt{3}}, \quad \rho = \sqrt{3J_2}, \quad I_1 = \mathrm{Tr}\,(\boldsymbol{\sigma}), \quad J_2 = \frac{1}{2}\mathbf{s}:\mathbf{s}, \tag{26}$$

$$Q_{\mathrm{MW}} = \rho^2 + B_g \rho + C_g \frac{I_1}{\sqrt{3}}, \tag{27}$$

$$B_g = \frac{2\left(\Omega_c f_c^{'}\right)\tan\psi - \sqrt{2}\left(\Omega_{tc} f_t\right)}{\sqrt{3\left(1-\sqrt{2}\tan\psi\right)}}, \quad C_g = \frac{B_g}{\sqrt{2}} + \frac{2\left(\Omega_{tc} f_t\right)}{\sqrt{3}}, \tag{28}$$

where ψ is the parameter of dilatancy, and Ω_{tc} is a function defined by Eq. (23).

Steel was described by the elastic-plastic Huber–Mises–Hencky (HMH) model with isotropic hardening, while corrosion products were described with the linear-elastic model.

2.7. Analysis of contact interactions

Contact calculations were performed using a modified Lagrange algorithm [38]. The contact between steel and concrete was modeled with CONTA174 and TARGE170 contact elements, taking into account the Columb friction model and the possibility of contact sliding [38]:

$$\tau_{\mathrm{lim}} = \mu P + c, \quad \|\boldsymbol{\tau}\| = \sqrt{\tau_1^2 + \tau_2^2} \leq \tau_{\mathrm{lim}}, \quad \|\boldsymbol{\tau}\| \leq \tau_{\max}, \tag{29}$$

where P is the force normal to the contact surface, τ_{lim} is the sliding limit, and $\tau_{\max}$ is the maximum allowable value of shear stresses.

3. Analysis of computational example

Using the proposed theoretical approach, calculations of the three-dimensional test element were performed. The obtained results were compared with the results of experimental studies presented in [23]. The reinforced concrete element analyzed in this paper, with dimensions of $100 \times 100 \times 80$ mm, was subjected to accelerated corrosion of the reinforcement using an electrolyzer (4 samples subjected to 20 V electric current, monitoring with a frequency of 60 s).

The computational analysis was performed using a unidirectionally coupled thermo(diffusion)-mechanical model available in ANSYS (the heat flow equation was treated as a diffusion equation). In the first step, the diffusion problem was analyzed with a defined mass source as a function of corrosion current intensity according to Eqs. (6) and (7) (source functions were determined using Mathematica and Excel software). In the next stage, a mechanical problem was analyzed, in which subsequent time increments took into account changes in the concentration of corrosion products and the coefficient of corrosion expansion of the corrosion product layer over time according to the relationships (15) and (16).

The code that performs the calculation was written in the ANSYS internal language APDL. The applied MW concrete model with HSD2 depending on the fracture energy is available in ANSYS from the level of APDL. For the purposes of comparative calculations, the FEM model of the test element presented in Fig. 2a was made. In Fig. 2b, the schematic diagram of the steel ring model of corrosion is shown, where the following designations were adopted: 1 – reinforcing steel; 2 – concrete; 3 – steel ring reflecting the increase in the volume of corrosion products; 4 – contact elements. As already mentioned in Sec. 2, the model was made as elastic-plastic with the contact: concrete MW model described by the relations (19)–(28), steel HMH model. Both the concrete and the steel reinforcing bar were made using eight-node SOLID185 solid elements, which were integrated using the full integration scheme [40]. The mutual interaction between the concrete cover and the corroding rebars was mapped using contact elements TARGE170 and CONTA174, assuming no possibility of separation of the contact area.

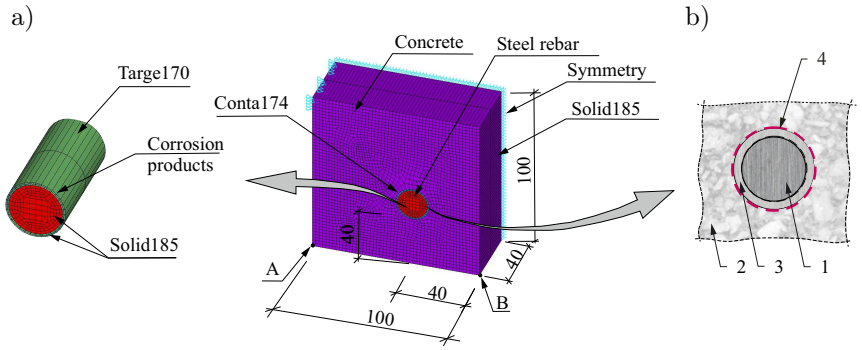

Fig. 2. Computer model (dimensions in mm): a) FEM model of the problem, b) schematic diagram of the steel ring model of corrosion products, description in the text.

The interactions of corrosion products with the concrete cover were achieved by assuming a steel ring with a width of 1 mm released from the reinforcing bar. The modeling scheme of the contact zone is shown schematically in Fig. 2b. The method of mapping corrosion products using a steel ring was adopted due to the stability and rapid convergence of such a solution. Detailed considerations on the different approaches to modeling corrosion of reinforcement can be found, e.g., in [41].

Comparative calculations in accordance with the unidirectionally coupled mechanical-diffusion model were referred to the results of experimental tests as well as to the results of mechanical calculations where the test element was loaded with an equivalent volumetric strain mapping the process of corrosion. The electrical parameters of the analyzed system (evolution of the current I function) were determined on the basis of the average value of the measurements obtained in [23] and are presented in Fig. 3. In addition, this figure shows

the averaged values of increase in volumetric strains used in the comparative mechanical analysis, representing the impact of reinforcement corrosion products. Parameters characterizing the increase of tensor of corrosion volumetric strains caused by reinforcement corrosion (14) were approved based on [23]: the porosity of the transition layer $\varepsilon = 0.55$, the effective electrochemical equivalent of iron $k_{\text{eff},0} = 0.006271$ (g/μA · year), the thickness of the transition layer $w_{ws} = 7.5 \cdot 10^{-3}$ cm, and the critical time $t_{cr} = 53.83$ h. The criterion for evaluating the results of computer tests was the agreement with the results of elongation of the element edge (distance between corner points A and B) in the FEM model, Fig. 2, with those obtained on the basis of experimental studies.

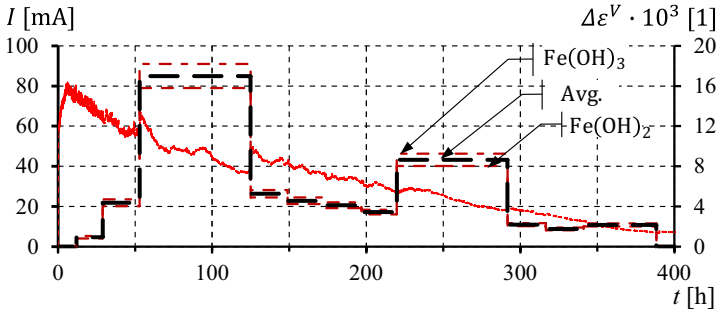

Fig. 3. Changes in the intensity of the electric current and substitute increases in volumetric strains in the analyzed test sample $\Delta\varepsilon_{\alpha\alpha}$, $\alpha = 1, 2$.

The diffusion model has been included in accordance with Eq. (6), where the mass source in the entire volume of the region subject to corrosion of the reinforcement (steel ring) has been defined. The part related to the mass flux has been omitted (to correctly declare the data, due to the software requirements, the mass diffusion coefficient of corrosion products $K = 1$ kg/m · s was declared). Diffusion flows were not included in the remaining areas. According to the relationship (1), the density of the skeleton was assumed as the sum of the partial densities of steel and concrete $\rho \approx \rho_0 = 2668$ kg/m^3 (1). The densities of the other components have been omitted.

The material parameters of the models used in the calculations for the MW concrete model in the elastic (including strength parameters) and inelastic (HSD2) ranges are presented in Tables 1 and 2.

Table 3 lists the material parameters adopted for the HMH material representing the reinforcing steel and the parameters adopted for the layer representing the mechanical impact of corrosion products. The steel-concrete interactions were accounted for by introducing contact (flexible model without separation of contact surfaces). The contact parameters were determined on the basis of the pre-code (Fédération Internationale du Béton-FIB 2013). The limit parameters

Table 1. Elastic and strength material parameters of concrete in the MW model.

Material parameters	Value
Initial Young's moduli, E_0 [MPa]	38280
Initial Poisson's coefficient, ν_0 [1]	0.2
Tensile strength, f_t [MPa]	3.99
Compressive strength, f_c [MPa]	56.4
Biaxial compressive strength, $f_b = 1.15 f_c$ [MPa]	64.86
Fracture energy, G_{ft} [N/m]	151

Table 2. Material parameters [38] describing the HSD2 hardening/softening model in relation to the MW material model.

Material parameters	Value
Plastic strain at uniaxial compressive strength, κ_{cm} [1]	0.00151
Plastic strain at transition from power law to exponential softening, κ_{cu} [1]	0.00175
Relative stress at start of nonlinear hardening, Ω_{ci} [1]	0.33
Residual relative stress at κ_{cu}, Ω_{cu} [1]	0.85
Residual compressive relative stress, Ω_{cr} [1]	0.2
Residual tensile relative stress, Ω_{tr} [1]	0.1
Dilatancy angle, ψ [deg]	20

Table 3. Elastic and strength material parameters of steel assumed in the HMH model, and elastic parameters of corrosion products (description in the text).

Material parameters	Value
Young's moduli, E [MPa]	200 000
Poisson's coefficient, ν [1]	0.3
Yield strength, f_y [MPa]	235

of contact slippage $\tau_{\max} = 2.5\sqrt{f_c}$ and cohesion for actions at the contact point between the reinforcing bar and concrete cover $c = 0.05\sqrt{f_c}$ were assumed. The values of the adopted model parameters are listed in Table 4.

Table 4. Material parameters defining the contact of steel and concrete (flexible contact).

Material parameters	Value
Friction coefficient, μ [1]	0.2
Cohesion coefficient, c [MPa]	0.375
Stiffness in normal direction, $k_{nn} \cdot 10^{-8}$ [MN/m^3]	1.8
Stiffness in tangential direction, $k_{tt} \cdot 10^{-8}$ [MN/m^3]	0.35
Maximum equivalent frictional stress (adhesion), $\tau_{\max}$ [MPa]	18.77

The calculations were made assuming two calculation situations, reflecting the composition of corrosion products on the reinforcing bar sidewall:

- Case I, corrosion products are a mixture of iron hydroxides II and III.
- Case II, a general approach assuming the formation of corrosion products with a complex composition consisting of a mixture of iron oxides and oxyhydroxides under the influence of electrolysis.

The calculations were carried out using a mechanical-diffusion model coupled in one direction (6) and (7). The analyzed decrease in iron ions and the related effective, uniform growth of corrosion products on the circumference of the rebar, determined on the basis of relations (15) and (16), were analyzed. The calculations were compared with the averaged results of displacements and crack widths (in the tested case, the average crack width approximately corresponds to the increase in the displacements of the test element) obtained on the basis of the tests carried out for four identical samples [23]. The test results were additionally compared with the calculation results obtained in the ANSYS program for the mechanical model using the MW model. In the course of further considerations, the designations EX E1, EX E2 were adopted for the experimental results concerning displacements (crack width) and MW B1 for the results of displacements obtained using the mechanical model, respectively, for the average composition of corrosion products consisting of iron hydroxides II and III ($Fe(OH)_2$ and $Fe(OH)_3$). The above-mentioned list of test results and analyzed models is shown in Table 5.

Table 5. List of results of experimental and model tests (indications and assumed composition of corrosion products).

Type of tests/concrete cover material model/type of hardening (softening)	Denotation	Corrosion products composition
Changes in the current intensity, I	EX E1	Real composition
Experimental study, cracks	EX E2	Real composition
Experimental study, displacement	EX E3	Real composition
MW/HSD2, mechanical model	MW B1	Avg. ($Fe(OH)_3$, $Fe(OH)_2$)

In case I, the subject of the calculations was a situation in which we assume the composition of corrosion products in the form of an averaged mixture of iron hydroxides II and III ($Fe(OH)_2$ and $Fe(OH)_3$) with the parameters $\alpha = 0.5725$ and $\vartheta = 2.165$ (for pure substances the parameters assumed were: a) for $Fe(OH)_2$: $\alpha = 0.622$, $\vartheta = 2.24$, b) for $Fe(OH)_3$: $\alpha = 0.523$, $\vartheta = 2.09$). Calculations were made for three calculation variants characterized by a variable time step of $\Delta t = 0.1$ h, $\Delta t = 0.5$ h and $\Delta t = 5$ h, respectively, and the parameter of the effective electrochemical equivalent of iron $k_{\text{eff}} = k_{\text{eff},0}$. The computational models used,

along with their compositions, the composition of corrosion products and time increment, are summarized in Table 6.

Table 6. List of calculation variants analyzed in case I.

Concrete cover material model/type of hardening (softening)	Denotation	Corrosion products composition	Time increment Δt [h]
MW/HSD2	MW 1	Avg. ($Fe(OH)_3$, $Fe(OH)_2$)	5
MW/HSD2	MW 2	Avg. ($Fe(OH)_3$, $Fe(OH)_2$)	0.5
MW/HSD2	MW 3	Avg. ($Fe(OH)_3$, $Fe(OH)_2$)	0.1

In case II, the parameters α and ϑ, depending on the magnitude of the electric current, were taken into account. The calculations were made here based on the calculation data available in [36]. Due to the large uncertainties of the parameters used in [23] to determine the displacements and crack width, the calculations were also performed for the modified value of the χ parameter. Deviations from the exact result were related to the method of evaluating the content of corrosion products in the vessel in which the sample was soaked and the method of performing the experiment (each optical measurement involved removing the element from the vessel). In the case of the electrochemical equivalent of iron, the uncertainty that could distort the result of the calculations arises from the assumption that the value of parameter k is constant, while in the case analyzed in this paper, this value, similarly to the parameters α and ϑ, depends on the electric current. The purpose of the calculations at this stage was to calibrate the parameters of the model, which allows to obtain calculation results similar to the experimental ones. Models referring to case II were also analyzed for three time steps $\Delta t = 0.1$ h, $\Delta t = 0.5$ h, $\Delta t = 5$ h, parameter k_{eff} equal to $k_{\text{eff}} = k_{\text{eff},0}$ and the coefficients of the impact of corrosion products on the concrete cover $\chi = 0.4$ and $\chi = 0.8$. The models for which the calculations were made are presented in Table 7.

Table 7. The list of calculation variants analyzed in case II.

Material model of the cover/type of hardening (softening)	Denotation	Corrosion products	Δt [h]	Parameter k_{eff}	Parameter χ
MW/HSD2	MW7	mixture	5	$k_{\text{eff},0}$	0.4
MW/HSD2	MW8	mixture	0.5	$k_{\text{eff},0}$	0.4
MW/HSD2	MW9	mixture	0.1	$k_{\text{eff},0}$	0.4
MW/HSD2	MW10	mixture	5	$k_{\text{eff},0}$	0.8
MW/HSD2	MW11	mixture	0.5	$k_{\text{eff},0}$	0.8
MW/HSD2	MW12	mixture	0.1	$k_{\text{eff},0}$	0.8

In case II, the composition of corrosion products was analyzed as a mixture of oxides and oxyhydroxides in the total mass of corrosion products. The percentage content of products in the electric current density range of $i = 50$–$300\ \mu A/cm^2$ was obtained experimentally [36]. Due to the fact that the values of the current density in the calculation example analyzed change in the range of $i \cong 0$–$2000\ \mu A/cm^2$, functions approximating the propagation of changes of products in the electric current density function (18) were introduced based on additionally adopted measurement points. These points were arbitrarily forecasted on the basis of the measured content of oxide/oxyhydroxide fractions and corresponded to the current density values $i = 1\ \mu A/cm^2$ and $i = 2000\ \mu A/cm^2$. An additional criterion here was the assumption of stabilizing the percentage content of oxides and oxyhydroxides for currents exceeding $300\ \mu A/cm^2$. The adopted coefficients approximating the functions are listed in Table 8.

TABLE 8. Parameters of functions approximating the percentage content of oxides $\xi_x = \ln(a_x i^{b_x})$ and oxyhydroxides $\xi_x = \exp\left(c_x i^{d_x}/e_x i^{f_x}\right)$.

Function	a_x	b_x	c_x	d_x	e_x	f_x
ξ_1, (FeO)	$\xi_1 = \xi_4 - \xi_3 - \xi_2$		–	–	–	–
ξ_2, (Fe_2O_3)	$\xi_2 = 0.55 \cdot (\xi_4 - \xi_3)$		–	–	–	–
ξ_3, (Fe_3O_4)	42	6.17	–	–	–	–
$\xi_4 = \sum_{k=1\ldots3} \xi_k$	$\xi_4 = 100\% - \xi_8$		–	–	–	–
ξ_5, ($\alpha - FeO(OH)$)	–	–	$\xi_5 = \xi_8 - \xi_6 - \xi_7$			
ξ_6, ($\beta - FeO(OH)$)	–	–	$\xi_6 = (\xi_8 - \xi_7) \cdot 0.7$			
ξ_7, ($\gamma - FeO(OH)$)	–	–	3.7	0.78	0.83	0.83
$\xi_8 = \sum_{k=5..7} \xi_k$	–	–	0.48	0.36	0.105	0.41

Graphical images of functions approximating the percentage content of (independent) fractions depending on the density of the corrosion current: iron oxide Fe_3O_4, oxyhydroxides $\gamma - FeO(OH)$, and the total amount of oxides and oxyhydroxides is shown in Fig. 4.

Additionally, in order to illustrate the impact of individual fractions on the composition of corrosion products, Fig. 5 presents the courses of changes in the percentage content of a) oxides and oxyhydroxides as a function of time: FeO, Fe_2O_3, Fe_3O_4 in Fig. 5a, b) oxyhydroxides $\alpha - FeO(OH)$, $\beta - FeO(OH)$, $\gamma - FeO(OH)$ in Fig. 5b, and finally c) the changes in parameters α and ϑ describing the relationship between the mass (density) of corrosion products and the mass (density) of iron ions (5) or the total assumed composition of the product mixture on Fig. 5c.

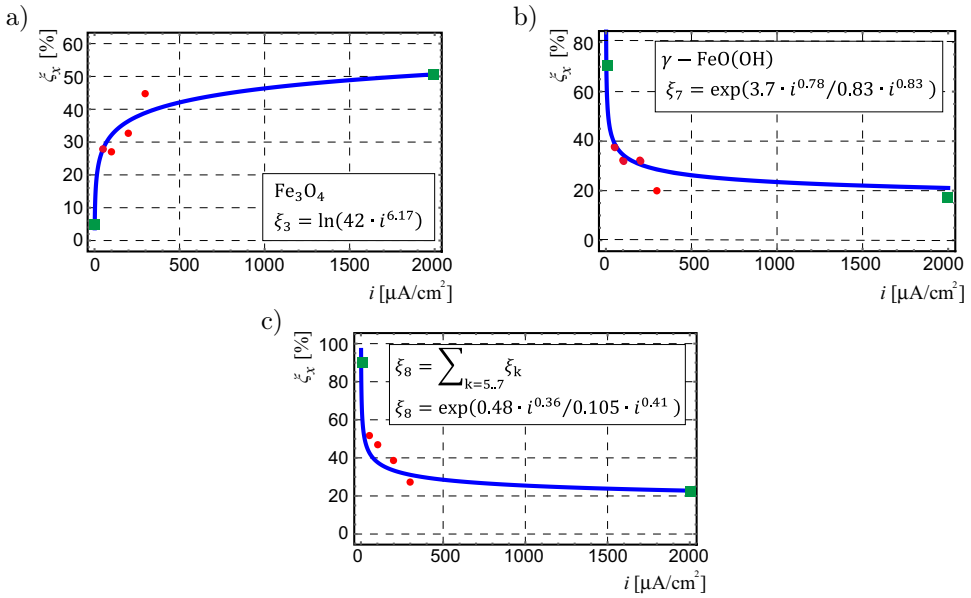

FIG. 4. Graphical images of functions approximating the percentage content of fractions in reinforcement corrosion products: a) Fe_3O_4, b) $\gamma - FeO(OH)$, c) total content of oxyhydroxides, $\alpha - FeO(OH)$, $\beta - FeO(OH)$, $\gamma - FeO(OH)$.

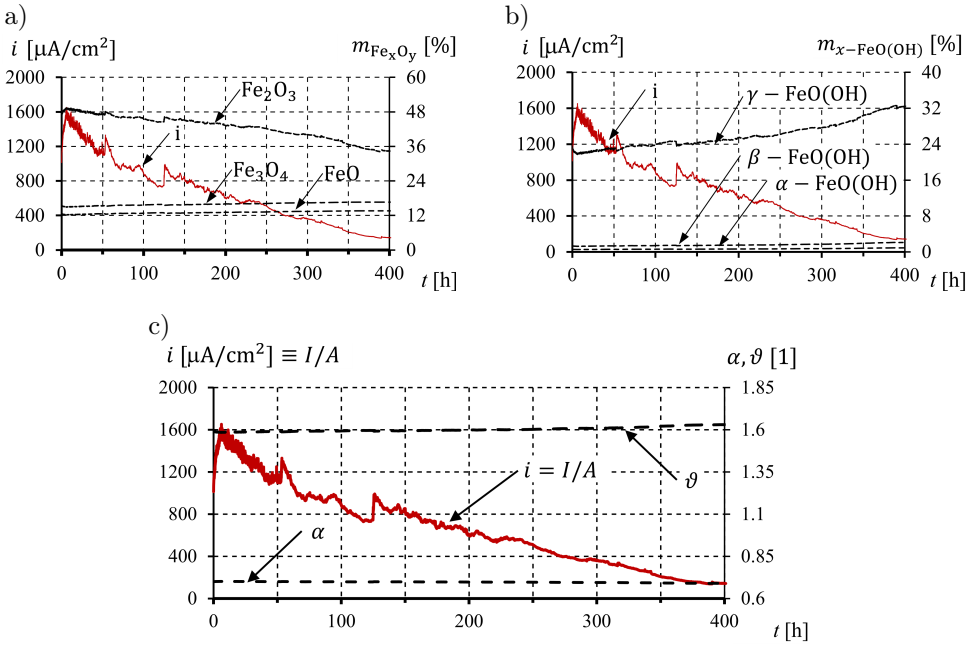

FIG. 5. Graphical image of percentage changes in a) percentage content of oxides, b) percentage content of oxyhydroxides, c) evolution of parameters α and ϑ as a function of electric current density (intensity) and time.

As a result of the calculations, graphical images were obtained describing changes in the displacements of edge points AB, Fig. 2. Calculation results obtained for a fixed composition of corrosion products, independent of the current intensity (mixture of iron hydroxides $Fe(OH)_2$ and $Fe(OH)_3$), in the case of diffusion-mechanical coupling are shown in Fig. 6. The results of calculations obtained for the determined parameters α and ϑ allow to obtain the results of elongation of the edge of the test element ΔL_{AB} (coinciding with the average width of the crack opening) that are consistent with the results of experimental tests. One can notice the convergence of the obtained calculation results obtained with the decrease of the time step increment. The calculation results, according to Table 5, were obtained for a series of time steps $\Delta t = 0.1$, 0.5 and 5 h. Some disturbances can be noticed at the initial stage of reinforcement corrosion $t \in (t_0, t_{cr})$. This state can be explained by the adopted time step and the adopted calculation parameters estimated in [23] and especially by the so-called initialization time t_0 and process critical time t_{cr}.

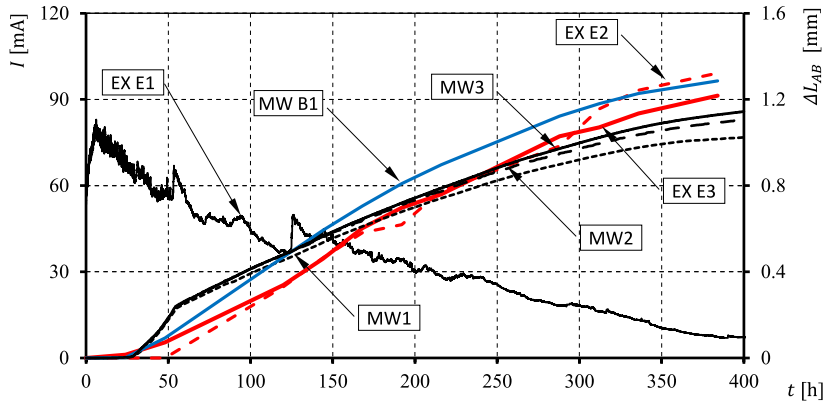

FIG. 6. Elongation of the edge of reinforced concrete cubes ΔL_{AB} as a result of rebars corrosion, corrosion products $Fe(OH)_2$ and $Fe(OH)_3$, fixed values of parameters α and ϑ.

The results of the calculations for the composition of corrosion products, which depends on the current intensity, are shown in Fig. 7. Additionally, in Fig. 8 the graphical image of the principal plastic strains in the time $t = 388$ h for the model MW12 (time step = 0.1 h, $k_{\text{eff}} = k_{\text{eff},0}$, $\chi = 0.8$, Table 7) was shown. In the case of calculations that assumed an arbitrary composition of reinforcement corrosion products dependent on the current density (intensity), the obtained results should also be considered satisfactory. As can be seen in Fig. 5c, the parameters α and ϑ, determined for the composition of corrosion products depending on the current density, differ from the values determined for the composition of corrosion products in the form of an averaged mixture of hydroxides II and III. In particular, these differences concern the parameter ϑ,

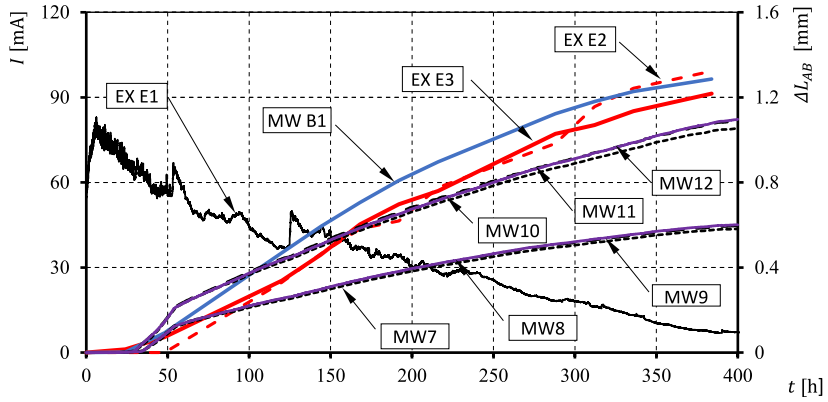

FIG. 7. Elongation of the edges of reinforced concrete elements ΔL_{AB} as a result of the rebars, corrosion products in the form of a mixture of oxides and oxyhydroxides, variables depending on the current density, parameters α and ϑ.

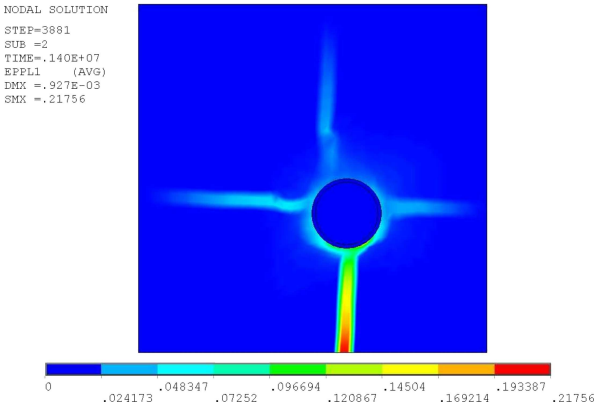

FIG. 8. Graphical image of principle plastic strains, model MW12, time $t = 388$ h.

which has a significant impact on the increase in the volume of products. In case II, this increase in volume is much smaller than in case I for the averaged mixture of the mentioned iron oxyhydroxides. The values of the discussed parameters also show, in the analyzed case, a relatively small variability over time for the test function of the corrosion current density. This variability is the result of the obtained composition of corrosion products as well as the range of variability of the measured current density values. The ϑ parameter in the analyzed calculation example varied between 1.59–1.63, while the value of the α parameter oscillated around the constant value of $\alpha = 0.69$. The solution obtained using the MW model was, in the analyzed case, stable and not very sensitive to the calculation step, which is probably due to a slightly different approach to the algorithm of the calculations. In the case of fixed parameters, the equivalent coefficient of material expansion was declared as a material constant, while in

the case of variable parameters, the calculations were carried out in a slightly different way by scaling the obtained values of corrosion product concentration.

4. Summary

The approach presented in the paper allows for a coherent way to analyze the problems of cover degradation in reinforced concrete elements in the field of reinforcement corrosion. It is possible, e.g., to analyze cases where corrosion products are mixtures of many chemical compounds, which are dependent on physical and chemical conditions. In addition, the approach allows for modeling the problems of both uniform and nonuniform corrosion on the circumference of the rebar.

Extremely important in the demonstrated model is the way of presenting the issues of forming corrosion products on the circumference of the rebar. The model allows not only (as it was formulated in this paper) to describe corrosion by mass sources but also to describe the loss of reinforcement and the formation of corrosion products by defining mass fluxes of these quantities. As a consequence of formulating the model in the form of thermodiffusion equations, it is also possible to include and interconnect other physical fields, such as the temperature field T, water content W, or the mass flux of chloride ions Cl^-.

The effectiveness of the model should be considered adequate despite slight discrepancies in the comparison to the experimental results in the initial phase of the corrosion process. In general, the model allows for satisfactory results, is convergent and stable, and can be used with very different media models, including mesoscopic models or those in which the pore structure is explicitly included.

Acknowledgments

This research project was financially supported by the National Centre for Research and Development, NCBR, Poland, the competition for research projects with the participation of scientists from Belarus entitled "Solidarity with scientists", Modeling the durability and degradation of reinforced concrete elements in conditions of reinforcement corrosion.

References

1. H. Böhni [Ed.], *Corrosion in Reinforced Concrete Structures*, Woodhead Publishing, 2005.
2. Z. Wang, W. Jin, Y. Dong, D.M. Frangopol, Hierarchical life-cycle design of reinforced concrete structures incorporating durability, economic efficiency and green objectives, *Engineering Structures*, **157**: 119–131, 2018, doi: 10.1016/j.engstruct.2017.11.022.

3. U. Angst, M. Büchler, On the applicability of the Stern–Geary relationship to determine instantaneous corrosion rates in macro-cell corrosion, *Materials and Corrosion*, **66**(10): 1017–1028, 2015, doi: 10.1002/maco.201407997.

4. Z.P. Bažant, Physical model for steel corrosion in concrete sea structures—theory, *Journal of the Structural Division, ASCE*, **105**(6): 1137–1153, 1979, doi: 10.1061/JS DEAG.0005168.

5. S.J. Pantazopoulou, K.D. Papoulia, Modeling cover-cracking due to reinforcement corrosion in rc structures, *Journal of Engineering Mechanics*, **127**(4): 342–351, 2001, doi: 10.1061/(ASCE)0733-9399(2001)127:4(342).

6. Y. Liu, R.E. Weyers, Modeling the time-to-corrosion cracking in chloride contaminated reinforced concrete structures, *ACI Materials Journal*, **95**: 675–681, 1998, doi: 10.14359/410.

7. A. Jamali, U. Angst, B. Adey, B. Elsener, Modeling of corrosion-induced concrete cover cracking: A critical analysis, *Construction and Building Materials*, **42**: 225–237, 2013, doi: 10.1016/j.conbuildmat.2013.01.019.

8. Y. Liu, *Modeling the Time-To-Corrosion Cracking of the Cover Concrete in Chloride Contaminated Reinforced Concrete Structures*, Ph.D. Thesis, Virginia Polytechnic Institute and State University, 1996.

9. A. Michel, B.J. Pease, M.R. Geiker, H. Stang, J.F. Olesen, Monitoring reinforcement corrosion and corrosion-induced cracking using non-destructive X-ray attenuation measurements, *Cement and Concrete Research*, **41**(11): 1085–1094, 2011, doi: 10.1016/j.cemconres.2011.06.006.

10. A. Michel, B.J. Pease, A. Peterová, M.R. Geiker, H. Stang, A.E.A. Thybo, Penetration of corrosion products and corrosion-induced cracking in reinforced cementitious materials: Experimental investigations and numerical simulations, *Cement and Concrete Composites*, **47**: 75–86, 2014, doi: 10.1016/j.cemconcomp.2013.04.011.

11. B. Wieczorek, T. Krykowski, Application of damage mechanics rules to evaluate the growth of corrosive deformations in transition layer [in Polish: Zastosowanie reguł mechaniki uszkodzeń do oceny wzrostu odkształceń korozyjnych w warstwie przejściowej], *Ochrona przed Korozją*, **60**: 5–8, 2017, doi: 10.15199/40.2017.1.1.

12. B. Martín-Pérez, *Service Life Modelling of R.C. Highway Structures Exposed to Chlorides*, Ph.D. Thesis, University of Toronto, 1999.

13. K. Maekawa, T. Ishida, T. Kishi, Multi-scale modeling of concrete performance, *Journal of Advanced Concrete Technology*, **1**(2): 91–126, 2003, doi: 10.3151/jact.1.91.

14. J. Ožbolt, F. Oršanic, G. Balabanić, M. Kušte, Modeling damage in concrete caused by corrosion of reinforcement: coupled 3D FE model, *International Journal of Fracture*, **178**: 233–244, 2012, doi: 10.1007/s10704-012-9774-3.

15. J. Ožbolt, F. Oršanić, G. Balabanić, Modeling pull-out resistance of corroded reinforcement in concrete: Coupled three-dimensional finite element model, *Cement and Concrete Composites*, **46**: 41–55, 2014, doi: 10.1016/j.cemconcomp.2013.10.014.

16. J. Ožbolt, F. Oršanić, G. Balabanić, Modelling processes related to corrosion of reinforcement in concrete: coupled 3D finite element model, *Structure and Infrastructure Engineering*, **13**(1): 135–146, 2017, doi: 10.1080/15732479.2016.1198400.

17. C. Cao, M.M.S. Cheung, Non-uniform rust expansion for chloride-induced pitting corrosion in RC structures, *Construction and Building Materials*, **51**: 75–81, 2014, doi: 10.1016/j.conbuildmat.2013.10.042.

18. C. Cao, M.M.S. Cheung, B.Y.B. Chan, Modelling of interaction between corrosion-induced concrete cover crack and steel corrosion rate, *Corrosion Science*, **69**: 97–109, 2013, doi: 10.1016/j.corsci.2012.11.028.

19. A. Chauhan, U.K. Sharma, Crack propagation in reinforced concrete exposed to non-uniform corrosion under real climate, *Engineering Fracture Mechanics*, **248**: 107719, 2021, doi: 10.1016/j.engfracmech.2021.107719.

20. L. Dai, D. Long, L. Wang, Meso-scale modeling of concrete cracking induced by 3D corrosion expansion of helical strands, *Computers and Structures*, **254**: 106615, 2021, doi: 10.1016/j.compstruc.2021.106615.

21. X. Fang, Z. Pan, A. Chen, Phase field modeling of concrete cracking for non-uniform corrosion of rebar, *Theoretical and Applied Fracture Mechanics*, **121**: 103517, 2022, doi: 10.1016/j.tafmec.2022.103517.

22. M. German, J. Pamin, FEM simulations of cracking in RC beams due to corrosion progress, *Archives of Civil and Mechanical Engineering*, **15**(4): 1160–1172, 2015, doi: 10.1016/j.acme.2014.12.010.

23. T. Krykowski, T. Jaśniok, F. Recha, M. Karolak, A cracking model for reinforced concrete cover, taking account of the accumulation of corrosion products in the ITZ layer, and including computational and experimental verification, *Materials*, **13**: 5375, 2020, doi: 10.3390/ma13235375.

24. Y. Auyeung, P. Balaguru, L. Chung, Bond behavior of corroded reinforcement bars, *ACI Materials Journal*, **97**(2): 214–220, 2000, doi: 10.14359/826.

25. C. Suwito, Y. Xi, The effect of chloride-induced steel corrosion on service life of reinforced concrete structures, *Structure and Infrastructure Engineering*, **4**(3): 177–192, 2008, doi: 10.1080/15732470600688699.

26. J. Ožbolt, G. Balabanić, G. Periškić, M. Kušter, Modelling the effect of damage on transport processes in concrete, *Construction and Building Materials*, **24**(9): 1638–1648, 2010, doi: 10.1016/j.conbuildmat.2010.02.028.

27. Y.Z. Wang, Y.X. Zhao, F.Y. Gong, J.F. Dong, K. Maekawa, Developing a three-dimensional finite element analysis approach to simulate corrosion-induced concrete cracking in reinforced concrete beams, *Engineering Structures*, **257**: 114072, 2022, doi: 10.1016/j.engstruct.2022.114072.

28. A. Zybura, *Degradation of Reinforced Concrete in the Corrosion Conditions* [in Polish: *Degradacja żelbetu w warunkach korozyjnych*], Dział Wydawnictw Politechniki Ślaskiej, Gliwice, 1990.

29. A.C. Eringen, G.A. Maugin, *Electrodynamics of Continua I: Foundations and Solid Media*, Springer, New York, NY, 1990, doi: 10.1007/978-1-4612-3226-1.

30. J. Kubik, *Thermodiffusion Flows in a Solid with a Dominant Constituent*, Ruhr-Universität Bochum, Bochum, Germany, 1985.

31. K. Wilmanski, *Continuum Thermodynamics*, World Scientific, Berlin, Heidelberg, 2008, doi: 10.1142/7052.

32. J. Lemaitre, J.-L. Chaboche, *Mechanics of Solid Materials*, Cambridge University Press, 1990.

33. T. Krykowski, Modeling of the cover damage caused by concrete reinforcement corrosion [in Polish: Modelowanie uszkodzenia otuliny wywołanego korozją zbrojenia w żelbecie], *Studia z Zakresu Inżynierii*, Nr 78, Polska Akademia Nauk, Komitet Inżynierii Lądowej i Wodnej PAN, Warszawa, 2012.

34. K. Wilmański, *Foundations of Phenomenological Thermodynamics* [in Polish: *Podstawy termodynamiki fenomenologicznej*], PWN, Warszawa, 1974.

35. B. Wieczorek, T. Krykowski, Application of damage mechanics rules to evaluate the growth of corrosive deformations in transition layer [in Polish: Zastosowanie reguł mechaniki uszkodzeń do oceny wzrostu odkształceń korozyjnych w warstwie przejściowej], *Ochrona przed Korozją*, **1**: 3–6, 2017, doi: 10.15199/40.2017.1.1.

36. W. Zhang, J. Chen, X. Luo, Effects of impressed current density on corrosion induced cracking of concrete cover, *Construction and Building Materials*, **204**: 213–223, 2019, doi: 10.1016/j.conbuildmat.2019.01.230.

37. P. Menetrey, K.J. Willam, Triaxial failure criterion for concrete and its generalization, *ACI Structural Journal*, **92**(3): 311–318, 1995, doi: 10.14359/1132.

38. ANSYS, *Material Reference*, Canonsburg, PA 15317, 2021.

39. P. Grassl, K. Lundgren, K. Gylltoft, Concrete in compression: A plasticity theory with a novel hardening law, *International Journal of Solids and Structures*, **39**(20): 5205–5223, 2002, doi: 10.1016/S0020-7683(02)00408-0.

40. ANSYS, *ANSYS Reference Manual*, Canonsburg, PA, USA, 2015.

41. K. Yurkova, T. Krykowski, Modeling of the formation of reinforcement corrosion products and their impact on damage of the concrete cover [in Polish: Modelowanie powstawania produktów korozji zbrojenia i ich wpływu na uszkodzenie otuliny betonowej], *Inżynieria i Budownictwo*, **78**(9–10): 410–413, 2022.

Received December 31, 2022; revised version April 17, 2023;
accepted May 10, 2023.